Intrazeolite Photochemistry. 17. Zeolites as Electron Donors: Photolysis of Methylviologen Incorporated within Zeolites

ARTICLE *in* THE JOURNAL OF PHYSICAL CHEMISTRY B · APRIL 1997

Impact Factor: 3.3 · DOI: 10.1021/jp9628850

Intrazeolite Photochemistry. 17. Zeolites as Electron Donors: Photolysis of Methylviologen Incorporated within Zeolites

Mercedes Alvaro,[†] Hermenegildo García,*[,†,‡] Sara García,[‡] Francisco Márquez,[‡] and J. C. Scaiano*[,§]

Departamento de Química, Universidad Politécnica, Apartado 22012, 46071 Valencia, Spain, Instituto de Tecnología Química CSIC-UPV, Universidad Politécnica, Apartado 22012, 46071 Valencia, Spain, and Department of Chemistry, University of Ottawa, Ottawa, Ontario, K1N 6N5, Canada

Received: September 19, 1996; In Final Form: January 27, 1997[⊗]

Methylviologen (MV^{2+}) has been adsorbed in a series of zeolites including alkaline ion faujasites (HNaY, LiNaY, NaY, KNaY, RbNaY, CsNaY, and NaX), Naβ, NaMor, and NaZSM-5 by ion exchange. Extra large pore aluminosilicate MCM-41 was also used. The resulting MV^{2+}-doped zeolites have been characterized by an array of analytical and spectroscopic techniques such as chemical analyses, X-ray photoelectron spectroscopy, thermogravimetry−differential scanning calorimetry, diffuse reflectance spectroscopy, and fluorescence, FT-IR, FT-Raman, and MAS ^{13}C NMR spectroscopies. Influence of the confinement and nature of the charge-balancing cation on the molecular properties of MV^{2+} resulted in shifts of the λ_{max} of the absorption band in the diffuse reflectance spectra from 270 to 280 nm for MV−NaX and 290 nm for MV−NaZSM-5 samples. In addition, changes of the relative intensities of the emission bands at 340 and 420 nm were also noted. The formation of the $MV^{\bullet+}$ cation radical as a persistent species by thermal treatment from the MV^{2+} ground state was not observed in any of the samples. In contrast, laser flash photolysis of these samples allowed in all cases the detection of $MV^{\bullet+}$ as a long-lived transient on the microsecond time scale. Formation of $MV^{\bullet+}$ was also observed by X-ray photoelectron spectroscopy. This constitutes the first firm experimental evidence that zeolites can behave as single electron donors. For MV−RbNaY and MV−CsNaY samples in outgassed sealed quartz cells, the photogenerated $MV^{\bullet+}$ is so long-lived that its diffuse reflectance spectrum and disappearance kinetics can be obtained by conventional diffuse reflectance spectroscopy. A relationship between the basic strength of the zeolite framework and the stability of photogenerated $MV^{\bullet+}$ has been established.

Introduction

The ability of zeolites to generate radical cations spontaneously upon adsorption of electron-rich organic compounds by single electron abstraction is by now firmly established.[1−12] Although the exact structure of the sites responsible for the electron acceptor ability of these microporous crystalline solids is still not completely established, a consensus is beginning to be reached that this property of zeolites is related to the presence of acid centers, the key question being the Brönsted or Lewis nature of the sites involved. In contrast, the reverse situation in which zeolites act as single electron donors for electron-deficient organic species is far less documented. In a review covering zeolites in electron-transfer processes, no published references were given, although such possibility was anticipated.[13]

In this context, during the laser flash photolysis of the xanthylium ion embedded within ZSM-5, we have previously observed an absorption at 340 nm in the time-resolved diffuse reflectance spectrum attributable to the xanthyl radical that would be generated by single electron transfer from the zeolite to the excited state of the cation.[14] However, this evidence was complicated by the concurrent T−T absorption of the triplet and by bleaching signals due to the ground state of the highly colored xanthylium ion. Thus, a spectrum corresponding exclusively to the xanthyl radical could not be obtained.

In the present work, we have prepared a wide and consistent series of zeolites containing methylviologen (MV^{2+}). The behavior of MV^{2+} as a powerful single electron acceptor in its excited state has been firmly established in solution.[15−24] In addition, the radical cation $MV^{\bullet+}$ generated after electron transfer has been characterized by several techniques in various media and a wealth of information is now available.[24−37] In particular, $MV^{\bullet+}$ can be unambiguously identified by its characteristic UV−vis spectrum consisting of an intense absorption at 390 nm and a broad band of medium intensity with a partially resolved structure centered at ∼600 nm.[38] Although our work was in progress, photoreduction of MV^{2+} exchanged in zeolites A, NaX, and NaY at 77 K has been reported.[24]

In this work, we have characterized an extensive series of MV^{2+}-doped zeolites by a combination of experimental techniques including thermogravimetry, X-ray photoelectron spectroscopy (XPS), diffuse reflectance spectroscopy (DR), and fluorescence, Raman, IR, and ^{13}C NMR spectroscopies. The samples were submitted to UV irradiation, and we have been able to establish unequivocally the formation of $MV^{\bullet+}$, both under reactive conditions in the submillisecond time domain for all the samples and in the absence of oxygen and moisture by conventional spectroscopic techniques in some cases. The aim of our work was to obtain conclusive experimental evidence that zeolites can also act as single electron donors and to establish a relationship between the physicochemical parameters of the zeolites and their ability as electron donors. Thus, we have established that in the same way that acidity of zeolites is

[†] Departamento de Química, Universidad Politécnica.
[‡] Instituto de Tecnología Química CSIC-UPV, Universidad Politécnica.
[§] Department of Chemistry, University of Ottawa.
[⊗] Abstract published in *Advance ACS Abstracts,* March 1, 1997.

S1089-5647(96)02885-4 CCC: $14.00

TABLE 1: Structures and Chemical Compositions of the MV^{2+}-Doped Aluminosilicates Prepared in This Work

sample	unit cell composition	unit cell composition after exchange with MV^{2+}	MV^{2+} content (mmol g^{-1})	loading of MV^{2+} per supercage
LiNaY	$Na_{27}Li_{26}Al_{53}Si_{139}O_{384}\cdot 50H_2O$	$Na_{27}Li_{20.05}(MV)_{2.8}Al_{53}Si_{139}O_{384}\cdot 166H_2O$	0.2103	0.35
NaY	$Na_{53}Al_{53}Si_{139}O_{384}\cdot 223H_2O$	$Na_{45.8}(MV)_{3.6}Al_{53}Si_{139}O_{384}\cdot 183H_2O$	0.2151	0.45
KNaY	$Na_8K_{45}Al_{53}Si_{139}O_{384}\cdot 175H_2O$	$Na_8K_{37.6}(MV)_{3.7}Al_{53}Si_{139}O_{384}\cdot 173H_2O$	0.2237	0.46
RbNaY	$Na_{14.5}Rb_{38.5}Al_{53}Si_{139}O_{384}\cdot 125H_20$	$Na_{14.5}Rb_{32.3}(MV)_{3.1}Al_{53}Si_{139}O_{384}\cdot 125H_2O$	0.1783	0.39
CsNaY	$Na_{20}Cs_{33}Al_{53}Si_{139}O_{384}\cdot 136H_2O$	$Na_{16.8}Cs_{28.8}(MV)_{3.8}Al_{53}Si_{139}O_{384}\cdot 136H_2O$	0.1984	0.47
HNaY	$Na_{31}H_{22}(AlO_2)_{53}(SiO_2)_{139}\cdot 144H_2O$	$Na_{26}H_{22}(MV)_{2.5}(AlO_2)_{53}(SiO_2)_{139}\cdot 136H_2O$	0.1524	0.29
NaX	$Na_{96}Al_{96}Si_{96}O_{384}\cdot 178H_2O$	$Na_{89.3}(MV)_{3.3}Al_{96}Si_{96}O_{384}\cdot 196H_2O$	0.1981	0.42
Nass	$Na_{4.6}Al_{4.6}Si_{60}O_{129}\cdot 22H_2O$	$Na_{2.8}(MV)_{0.9}Al_{4.6}Si_{60}O_{129}\cdot 25H_2O$	0.2038	0.45
NaMor	$Na_{6.5}Al_{6.5}Si_{41.5}O_{96}\cdot 23H_2O$	$Na_{4.6}(MV)_{1.9}Al_{6.5}Si_{41.5}O_{96}\cdot 23H_2O$	0.2784	
NaZSM5	$Na_{4.6}Al_{4.6}Si_{92}O_{193}\cdot 14H_2O$	$Na_{1.4}(MV)_{1.6}Al_{4.6}Si_{92}O_{193}\cdot 18H_2O$	0.2603	
HMCM41	$H_7Al_7Si_{95}O_{204}\cdot 38H_2O$	$H_{3.8}(MV)_{1.6}Al_7Si_{95}O_{204}\cdot 38H_2O$	0.2147	

related to their single electron acceptor ability, the basicity of the framework strongly influences the electron donor behavior of zeolites.

Results and Discussion

Preparation and Characterization of the MV^{2+}-Doped Zeolites. To encompass the widest range of chemical compositions and topologies, we have employed medium pore size zeolites (ZSM-5), as well as large pore zeolites of monodirectional (mordenite), bidirectional (β), and tridirectional (X and Y) topologies.[39] We have also included extra-large pore aluminosilicate MCM-41[40−42] to explore possible confinement effects when there is a tight fit of MV^{2+} on zeolites of smaller micropore dimensions. In addition, we have included a series of alkaline metal ion-exchanged Y zeolites to properly address the influence of basicity[43−53] on the ability of these materials as single electron donors, as well as the stability of the resulting $MV^{\bullet+}$.

Amorphous silica was not used, since two recent reports have studied the photolysis of MV^{2+} adsorbed on this nonmicroporous solid material.[32,37] We note that the ion exchange capacity of silica should be ideally zero, while in practice, it is very low owing to some impurities and defects. In contrast, in the case of zeolites, the different valence between silicon and aluminum introduces negative charges in the lattice that require the presence of charge-balancing cations (one monovalent cation per each framework aluminum) to satisfy the electroneutrality of the solid.[54−56] The ionic nature of the bond between the compensating cation and the lattice allows ion exchange without any alteration of the crystalline structure. Therefore, the amount of MV^{2+} incorporated in our zeolites (about 0.2 mmol of MV^{2+} per gram of zeolite; see Table 1) is 2 orders of magnitude higher than what can be adsorbed on silica by ion exchange (10^{-3} mmol of MV^{2+} per gram of silica).[32]

To obtain alkaline metal-exchanged Y zeolites, the commercial NaY sample was submitted to exhaustive ion exchange with alkaline ions before proceeding with the adsorption of MV^{2+}. In these cases, chemical analyses were performed before and after the incorporation of MV^{2+}. When there are two different cations in the supercage (Na^+ and an alkaline ion), this procedure has allowed us to establish which cation is preferentially exchanged by MV^{2+}. In general, we find that exchange of the second alkaline metal ion is preferred (see Table 1).

Doping of zeolites with MV^{2+} was carried out by stirring at room-temperature aqueous solutions of $MVCl_2$ in the presence of the corresponding alkaline ion form of the zeolite, except for MCM-41 for which an as-synthesized sample after calcination was used. Purposely, we also submitted a sample of HNaY to doping with MV^{2+}.

Table 1 summarizes the chemical composition of the MV^{2+}-doped zeolites prepared. The percentages of ion exchange were determined by atomic absorption spectroscopy of the remaining alkaline metal ion as well as combustion chemical analysis (C and N) of MV^{2+}.

In the case of zeolite Y, taking into account its high aluminum content, it would be possible to exchange up to a maximum of two MV^{2+} per supercage (corresponding to 1.76 mmol of MV^{2+} per gram of Y zeolite, approximately). Therefore, and also in view of the precedents in the literature,[13,57−62] no problems were anticipated during the ion exchange. However, taking into account the high Si/Al ratio of NaZSM-5 and MCM-41, and hence, their low ion exchange capacity (ZSM-5, 3.7×10^{-1}; MCM-41, 5×10^{-1} mmol of $MV^{2+} \times g^{-1}$), and the fact that the negative centers of the lattice associated with the random distribution of Al will be further apart, we were concerned with the possibility that some monopositive $MVCl^+$ ion pairs could be introduced during the exchange. For polyvalent metal ions, it is known that ion exchange with their complexes with anionic ligands can occur, each cation thus compensating for only one negative charge of the lattice.[63] Since the presence of chloride greatly influences the photochemical behavior of MV^{2+} on silica and other solids,[32] it is necessary to determine the total absence of Cl^- in our zeolitic samples. Otherwise, the possibility that upon excitation an electron transfer from Cl^- to MV^{2+} would occur could invalidate our results.

To determine the content of Cl^-, we performed XPS analyses of the MV−NaZSM-5 and MV−MCM-41 samples. It is well established that this technique is highly sensitive to the presence of chloride on the outer surface of the particle that is readily characterized by its 2p electron band at 199 eV. No Cl^- could be detected in any of these two samples. On the other hand, the samples turned blue, indicating the formation of $MV^{\bullet+}$ during X-ray excitation. Since the XPS sample chamber is under ultrahigh vacuum ($< 5 \times 10^{-9}$ Torr), no change in the color (as would have been expected if oxygen was present) could be observed for several hours after X-ray exposure.

The diffuse reflectance spectra of the samples showed a single absorption band around 270 nm. This absorption is much broader and a little shifted from that of MV^{2+} in aqueous solution. No significant λ_{max} shift of this band was noticed for the whole series of Y zeolites exchanged with alkaline metal ions (Figure 1A). In contrast, the samples MV−NaX and MV−NaZSM-5 exhibited a shift in λ_{max} that appeared at 280 and 290 nm, respectively (Figure 1B). These changes probably reflect changes in the polarity of the internal voids, differences in the planarity of the rings, and/or molecular orbital distortions owing to the confinement in a restricted space.[64−67] In this context, we have previously performed molecular modeling of the planar and orthogonal conformations of MV^{2+} inside the channels of ZSM-5 and found that the repulsive overlap of the

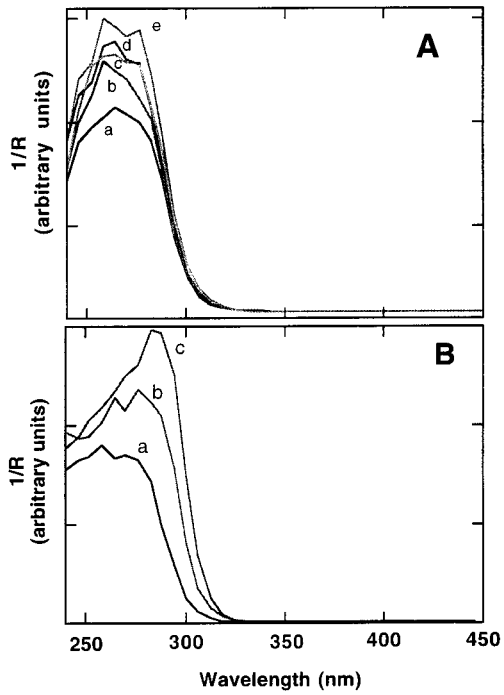

Figure 1. Diffuse reflectance spectra (1/*R*) of MV^{2+}-doped zeolites. Part A shows spectra of (a) MV-LiNaY, (b) MV−NaY, (c) MV−KNaY, (d) MV−RbNaY, and (e) MV−CsNaY with λ_{max} around 270 nm. Part B shows spectra of (a) MV−Naβ (λ_{max} = 270 nm), (b) MV−NaX (λ_{max} =280-nm), and (c) MV−NaZSM-5 (λ_{max} = 290 nm) with shifts in λ_{max}. For the sake of clarity, the latter spectra have been normalized.

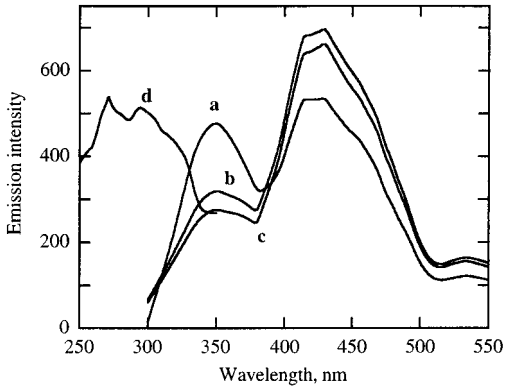

Figure 2. Emission spectra (λ_{exc} 280 nm) of MV−LiNaY (a), MV−RbNaY (b), and MV−CsNaY (c) recorded under the same conditions as in Figure 1. Trace d corresponds to the excitation spectrum of MV−CsNaY with the emission monitored at 440 nm and shows the onset at 330 nm and λ_{max} at 295 nm.

host−guest van der Waals atomic radii was lower when a planar conformation of the two rings of MV^{2+} is achieved.[68]

Although MV^{2+} does not fluoresce in solution,[69] it has been observed that MV^{2+} emits at 340 nm in the interlamellar region of layered smectite and montmorillonite clays.[70,71] We have already reported on the fluorescence of MV^{2+}-doped NaY, NaMor, and NaZSM-5, consisting of two bands at 340 and 420 nm.[68] We have now expanded these luminescence measurements and observed that there is a relationship between the nature of the accompanying alkaline metal ion of Y zeolite and the relative intensity of these two bands (Figure 2). Excitation spectra indicate that there are two emitting species with different absorption spectra: that which is responsible for the 340 nm emission has a sharp absorption at 282 nm, while the excitation spectrum of the second species obtained by monitoring at 420 nm is much broader with the onset at ∼330 nm. By using

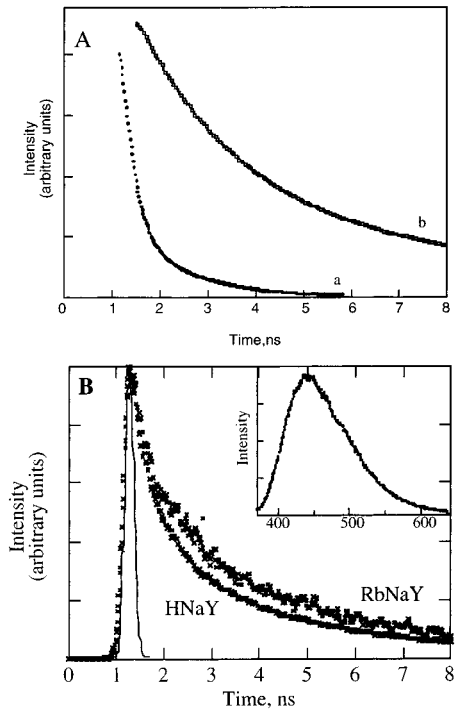

Figure 3. (A) Normalized fluorescence decays of MV−NaZSM-5 monitored at 350 nm (curve a) and 460 nm (curve b) after 266 nm laser excitation. (B) Fluorescence decay profiles of MV−HNaY and MV−RbNaY monitored at 420 nm obtained after 355 nm laser excitation. The continuous line shows the *instrument response function*, a combination of the laser pulse and the instrumental response. The insert of part B corresponds to the emission spectrum of MV−HNaY 10 ns after laser excitation (355 nm, 35 ps, 1 mJ), showing λ_{max} at 425 nm.

picosecond laser techniques, we have been able to record the time-resolved decay of this emission for some MV^{2+}-doped zeolites. Figure 3 shows that the fluorescence lifetimes of both emitting species are in the nanosecond range, being much shorter-lived the species responsible for the 320 nm fluorescence. In addition, the decay kinetics are also influenced by the nature of the associated charge-balance cation and the zeolite structure.

It is known that the basicity of zeolites increases as the ionic radius of alkaline charge-balancing cation or the framework Si/Al ratio increases. Thus, the stronger basicity of zeolites has been found for Cs^+-exchanged X and Y faujasites.[43,44,46] Interestingly, the stronger the basicity of the zeolite framework, the more intense is the emission at 420 nm. A reasonable explanation to account for the influence of the alkaline ion on the intensity of the 420 nm emission would be that the species responsible for this fluorescence is the population of MV^{2+} strongly complexed with the basic sites of the lattice. It has been found in solution that complexation of MV^{2+} with organic carboxylates leads to the broadening of the absorption spectrum with shifting of its λ_{max}, both facts agreeing with our observation for MV^{2+}-doped Y zeolites.[72]

Thermogravimetry coupled with differential scanning calorimetry (TG−DSC)[73] provides useful information on the thermal stability and temperature decomposition of MV^{2+} adsorbed within zeolites. Figure 4 shows the TG−DSC profiles for MV−NaMor, which is the sample for which the general behavior is more clearly seen. The other samples followed a similar pattern, although the TG−DSC profiles were smoother depending on the zeolite. Thus, after the initial loss of coadsorbed water at temperatures below 100 °C, differential calorimetry reveals the occurrence of one exothermic process peaking at 533 °C that

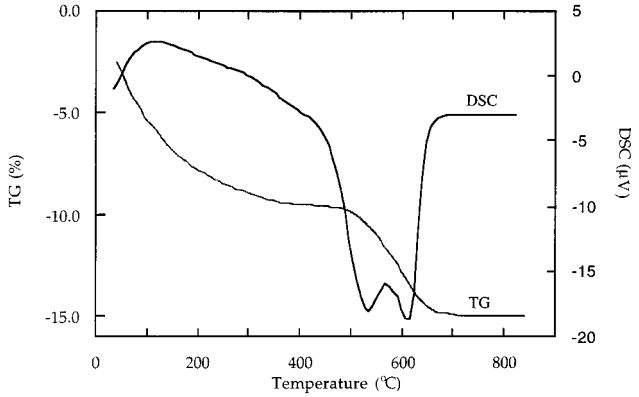

Figure 4. Thermogravimetric (TG, left axis) and differential scanning calorimetric (DSC, right axis) profiles of the MV−NaMor obtained in an air stream.

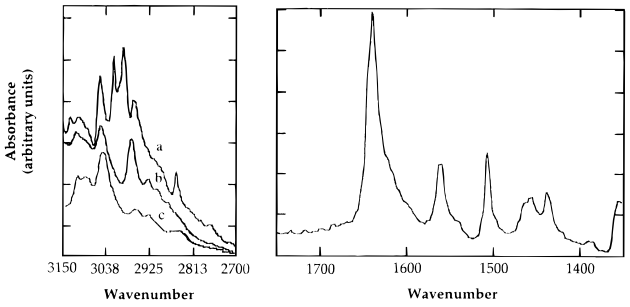

Figure 5. (Left) C−H stretching region of the FT-IR spectra of $MVCl_2$ in a KBr disk (a) and MV−NaY recorded at room temperature after outgassing (10^{-2} Pa) at room temperature (b) and at 200 °C for 1 h (c). Note the decrease in the intensity of the characteristic CH_3 bands below 3000 cm^{-1}. (Right) Aromatic region of the IR spectrum of MV−NaMor showing the characteristic absorption bands due to MV^{2+}.

is not accompanied by a concomitant loss of weight. The total desorption of the organic material takes place at higher temperatures, typically around 670 °C, concomitant with a second exothermic peak in DSC at 610 °C.

We were interested in understanding the nature of the transformation responsible for the first exothermic reaction occurring at 533 °C because it would shed some light on the presence of possible adventitious degradation products if the samples are thermally manipulated at high temperatures. For this purpose, we heated a MV−NaMor sample at 400 °C for 2 h in an oven under reduced pressure, and then the solid sample was dissolved using concentrated HF and extracted with dichloromethane. GC−MS analysis of the extract revealed the presence of significant amounts of 4,4′-bipyridine, which was confirmed by comparison with an authentic sample. Therefore, we tentatively attribute the exothermic reaction observed in the DSC curve to demethylation of MV^{2+}. In situ FT-IR spectroscopy also provided a direct confirmation of this process. The only strong absorption bands in the IR of dehydrated zeolites are those corresponding to OH groups in the 3800−3500 cm^{-1} region as well as the Si−O and Al−O stretching vibrations around 1050−950 cm^{-1}. Therefore, they do not interfere in the region characteristic of the main organic functional groups and allow the direct observation of the organic guests incorporated within the internal voids. We have recorded room-temperature IR spectra of MV^{2+}-doped zeolites after successively outgassing under vacuum at increasing temperatures for periods of 1 h. Although the aromatic region of the spectra of MV^{2+}-doped zeolites recorded after treatment at temperatures below 100 °C agree with the IR spectrum of $MVCl_2$ obtained in a KBr disk (except for the presence of some residual water), we observe remarkable variations after treatment of the samples at 200 °C. In addition, the C−H stretching region of IR spectra of MV^{2+}-doped zeolites does not exactly coincide with a pure sample of $MVCl_2$. This may probably reflect differences in the CH_3 vibrations when MV^{2+} is interacting with the zeolite network or when MV^{2+} is in the lattice of pure $MVCl_2$ crystals. Notably, the intensity of the bands characteristic of the methyl groups[74] at around 2960 and 2880 cm^{-1} was greatly diminished. We interpret these differences as an indication that *N*-demethylation of the heterocycle has occurred to a large extent when heating the samples at 200 °C under vacuum. This interpretation is in good agreement with the exothermic process observed in the TG−DSC analyses under atmospheric pressure in an air stream. Figure 5 shows some selected IR spectra of zeolites containing MV^{2+}.

The IR spectroscopic study is somewhat complicated by the presence of coadsorbed water in the samples. TG analyses established that the amount of water in our samples can be as high as 15 wt %. Since water exhibits strong bands in the IR, and particularly at 1640 cm^{-1}, the IR spectra of our samples recorded directly without any thermal treatment that could disturb the organic guest were generally dominated by the intense absorption bands due to H_2O. In contrast, water does not absorb significantly in Raman spectroscopy, where water can be used even as solvent.[75] IR spectroscopy proved the presence of MV^{2+} as the sole detectable organic material. In addition, we obtained Raman spectra of our samples. We wanted to ascertain the purity of MV^{2+} after adsorption on the zeolites by all available techniques to rule out impurities that could be responsible for the shifts in the diffuse reflectance spectra, the luminescence properties of our samples, or the single electron-transfer processes that we describe below.

The Raman spectra of MV^{2+}, $MV^{\bullet+}$, and related compounds have been the subject of intensive studies in the literature.[32,75−77] Complete assigment of the Raman bands to specific vibrational modes has been reported, thus making Raman spectroscopy a highly valuable technique in our case. As shown in Figure 6, the Raman spectra of MV^{2+} within zeolites match perfectly its spectrum in solution. No other peaks attributable to adventitious material present on untreated doped samples were observed.

MAS ^{13}C NMR spectra of MV−NaX and MV−NaY were also recorded. The spectra show the presence of four different types of carbons, compatible with the structure of MV^{2+}, although no significant changes in their chemical shifts were observed compared to those in aqueous solutions. However, the low sensitivity inherent in solid-state NMR and the broadness of the peaks severely limit its utility as an analytical technique. The poor resolution of the ^{13}C NMR peaks could be due in part to the interaction of the organic guest with quadrupolar aluminum, owing to the high aluminum content of faujasites, and/or may also reflect a wide distribution of the guest molecules among various locations in the crystalline structure of the zeolite.

Photolysis of MV^{2+}-Doped Zeolites. In none of the MV^{2+}-doped zeolites was the development of the characteristic blue color of $MV^{\bullet+}$ observable on standing after preparation. Furthermore, heating of sealed samples at temperatures below 200 °C does not lead to any detectable formation of $MV^{\bullet+}$. Therefore, no spontaneous single electron transfer from the zeolitic framework to MV^{2+} in its ground state was observed.

Photolysis of the MV^{2+} adsorbed within zeolites was carried out using either laser flash time-resolved techniques[78] on a microsecond time scale for septum-capped cells or conventional lamp irradiation of sealed quartz cells previously outgassed at room temperature under 10^{-2} Pa for 5 h. We have previously established[79] by monitoring the monomer and excimer emission of pyrene adsorbed on NaY during the aging of the samples

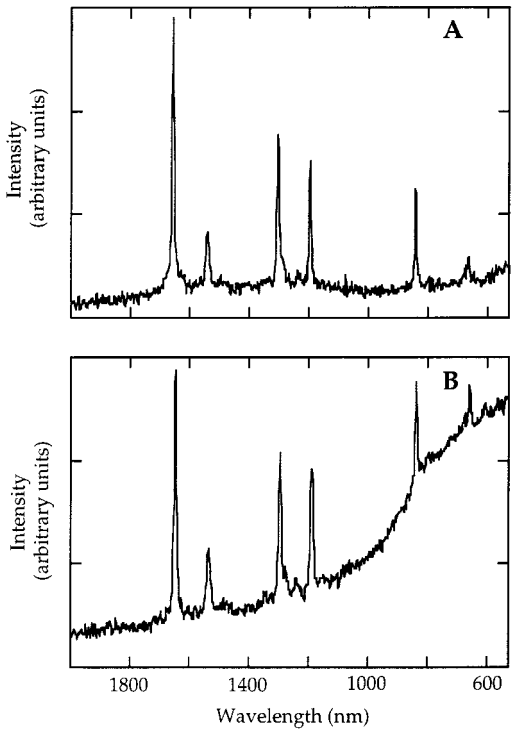

Figure 6. Raman spectra of $MVCl_2$ in aqueous solution (A) and in MV−NaY samples (B). In the latter case, the powder was not submitted to outgassing or thermal treatment.

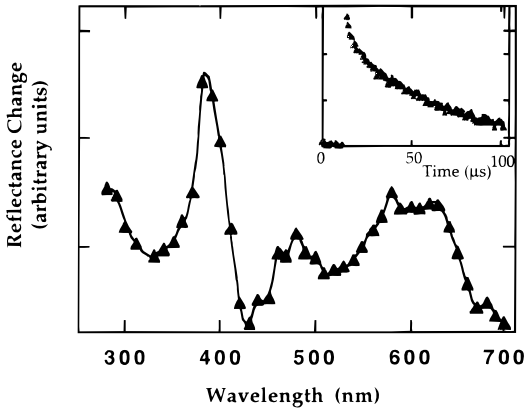

Figure 7. Transient diffuse reflectance spectrum ($\Delta J/J_o$) of the MV−HNaY sample recorded 9.6 μs after 266 nm laser flash excitation. The inset shows the decay of $MV^{\bullet+}$ monitored at 390 nm. The absorption bands at about 380 and 600 nm correspond to the monomer $MV^{\bullet+}$, while the band at 490 nm is due to the dimer.

that capping the cells with septa cannot fully prevent the influence of the air and ambient moisture on zeolites during the laser flash experiments. Only sealing of the cells guarantees that no oxygen will regain access during the irradiation procedure.

In contrast to the behavior of MV^{2+} in its ground state, time-resolved diffuse reflectance following laser flash photolysis systematically allowed the observation of $MV^{\bullet+}$ independently of the structure of the aluminosilicate, or of the nature of the charge compensating cation. In most cases, the time-resolved diffuse reflectance spectrum following 266 nm laser excitation matches perfectly the reported spectrum of $MV^{\bullet+}$ in solution. In some faujasite samples we observed the presence of an additional band at 490 nm that can be attributed to the $MV^{\bullet+}$ dimer. This absorption is especially important for the MV−HNaY sample (Figure 7). Dimerization of $MV^{\bullet+}$ is a well-known process in solution, and the dimer is characterized by a

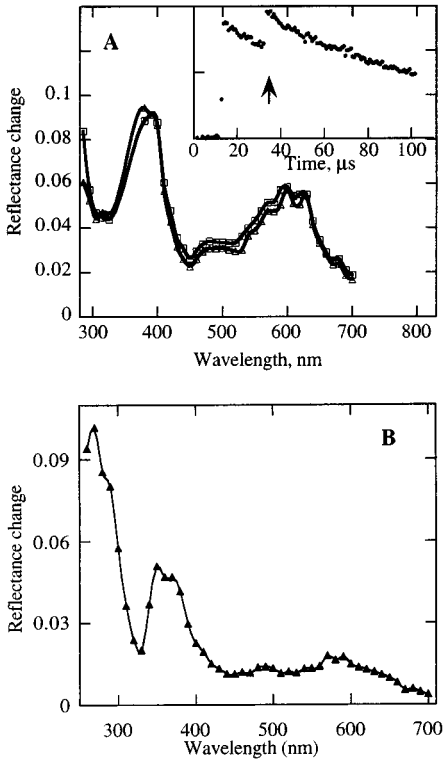

Figure 8. (A) Time-resolved diffuse reflectance spectra ($\Delta J/J_o$) recorded for MV−LiNaY upon 266 nm excitation before (△) and after (□) firing a second laser at 355 nm. The two laser flashes have been delayed by 30 μs. Note that both spectra are coincident, but the intensity increases after the second laser flash, showing that additional $MV^{\bullet+}$ has been generated. The inset shows the transient decay monitored at 570 nm, and the arrow indicates when the second laser has been fired. (B) Transient diffuse reflectance of MV−LiNaY recorded 80 μs after 355 nm excitation showing the presence of an absorption at 280 nm corresponding to the recovery of the MV^{2+} ground state.

band around 500 nm.[38,80−85] As could be anticipated according to a much more restricted reaction cavity, this dimer formation could not be observed for the MV−NaZSM-5 sample even though its loading level is similar to those of the other samples (see Table 1).

It is noteworthy that the same $MV^{\bullet+}$ spectrum could also be recorded upon 355 nm laser excitation of the samples. Even employing the two-laser two-color (266 plus 355 nm) technique[86] resulted in the additional generation of $MV^{\bullet+}$ after the second pulse (Figure 8). As we have already mentioned, 355 nm ensures the selective excitation of the chromophore responsible for the 420 nm emission. Our experiments demonstrate that this species also generates efficiently $MV^{\bullet+}$ as the sole detectable transient, thus reinforcing the prior interpretation that the most reasonable assignment for these species is a MV^{2+}-zeolite complex and not due to adventitious impurities.

The $MV^{\bullet+}$ radical cation generated by laser excitation showed a time-resolved decay in all samples examined. A growing of the band at 270 nm suggests that back-electron transfer to regenerate MV^{2+} is one of the main decay pathways (compare parts A and B of Figure 8). However, the disappearance kinetics on the microsecond time scale are too slow to allow accurate measurements of lifetimes in the different zeolites using a nanosecond laser flash setup. Thus, variable levels of residual absorption are observed in all the decay traces even at long time scales. Nevertheless, we noticed that there is a definite influence of the zeolitic environment on the disappearance of $MV^{\bullet+}$. Selected decays showing the variations observed depending on the nature of the alkaline ion and crystalline structure are presented in Figure 9.

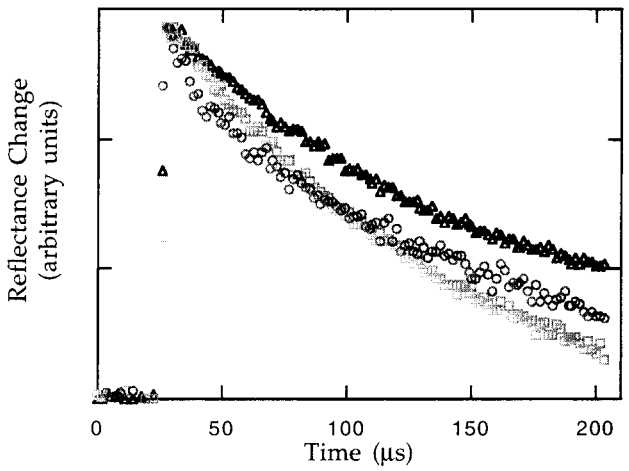

Figure 9. Normalized transient decays of $MV^{\bullet+}$ monitored at 570 nm after 266 nm excitation of MV−NaX (○), MV−NaMor (□), and MV−NaZSM-5 (△). Note that for MV−NaX, the initial part of the decay is much faster than the rest, suggesting that there are two different decay regimes.

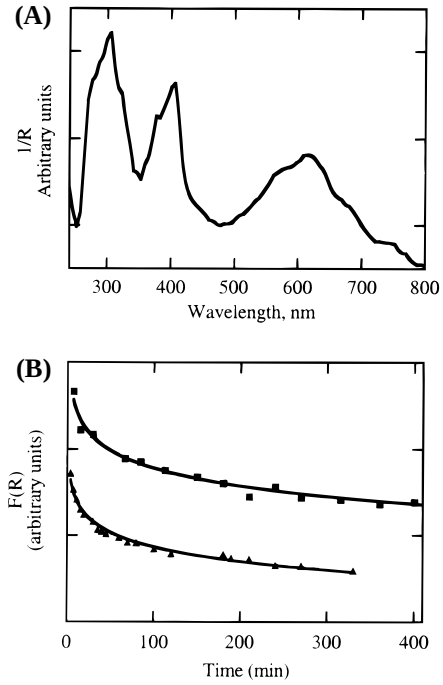

Figure 10. (A) Diffuse reflectance spectrum (1/*R*) of a MV−CsNaY sample after 30 min of lamp irradiation (125 W medium-pressure Hg) recorded using a conventional spectrophotometer. (B) Decay of the intensity as a Kubelka−Munk function [*F*(*R*)] of the 390 nm band for MV−CsNaY (■) and MV−RbNaY (△) samples after simultaneous lamp irradiation (30 min) followed by using a conventional spectroscopy.

Samples submitted to laser flash experiments in septum-capped cells remain generally white or develop a light-yellowish tint after exposure to a large number of laser pulses. The same lack of visible blue $MV^{\bullet+}$ occurs for the majority of the samples when the irradiation was performed by low-intensity lamp irradiation in sealed quartz cells. In contrast, when MV^{2+} is incorporated in RbNaY and CsNaY zeolites, the samples became blue and conventional diffuse reflectance spectra showed the presence of $MV^{\bullet+}$. The spectrum for MV−CsNaY is presented in Figure 10A and shows the presence of the $MV^{\bullet+}$ radical cation together with unreacted MV^{2+}. Assuming that the relative extinction coefficients of the species adsorbed are similar to those reported in solution, a quantitative estimation of the efficiency of the single electron-transfer process for each zeolite can be made. Notably, the blue color faded over time and the samples became white after several hours. The loss of color was much faster in RbNaY than in CsNaY ($F(R)$ for $MV^{\bullet+}/MV^{2+}$ is 0.31 and 0.14 for MV−CsNaY and MV−RbNaY, respectively). Conventional diffuse reflectance proved to be appropriate for following the disappearance kinetics of $MV^{\bullet+}$ under these conditions. Figure 10B shows that the decays were very dependent on the nature of the charge-balancing cation of the zeolite. The crystalline structure of the zeolite must also play a role. In fact, we also observe that MV−NaZSM-5 became blue during the irradiation, but the color disappeared after a few minutes, too fast to be followed conveniently with this technique.

SCHEME 1

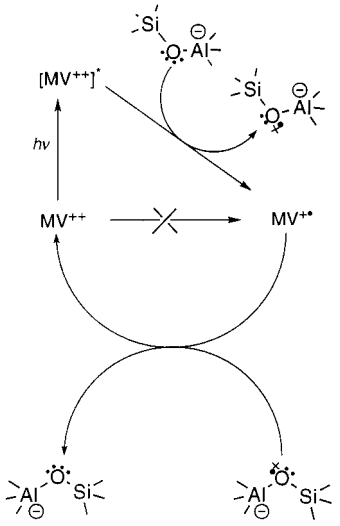

The combination of the information obtained by laser flash photolysis establishing that $MV^{\bullet+}$ is photochemically generated in all the samples and the fact that lamp irradiation only allows characterization of $MV^{\bullet+}$ in the more basic RbNaY and CsNaY indicates that it is not only the single electron-transfer step but also the $MV^{\bullet+}$ decay dynamics that are dependent on the nature of the zeolite. A likely rationalization is that the major pathway for the disappearance of $MV^{\bullet+}$ would be back-electron transfer from $MV^{\bullet+}$ to the radical center in the zeolite to regenerate MV^{2+} in its ground state plus the oxygen lone pair of the lattice. The higher the electron density on the oxygen acting as electron donor, the slower the anticipated rate of back-electron transfer. Therefore, the stability of $MV^{\bullet+}$ in a series of zeolites would follow the same order as their basic strength, as is in fact observed.

A reasonable rationalization of the processes occurring after light excitation is outlined in Scheme 1. Thus, absorption of a photon promotes MV^{2+} to its excited state from which it abstracts one electron from the oxygens of the framework, giving rise to an oxygen radical center and $MV^{\bullet+}$. This species then decays by reaction with coadsorbed water or oxygen or through back-electron transfer. In the latter case, MV^{2+} would be reformed.

Taking into account the $0 \rightarrow 0$ excitation energy for MV^{2+} ($\Delta E_{0,0} = 89$ kcal mol^{-1}) that can be approximately obtained from the comparison of our absorption and emission spectra and the reported oxidation potential of −0.78 V versus SCE for ground-state MV^{2+} in related zeolites,[61] it is possible to estimate the reduction potential of $[MV^{2+}]^*$ in its singlet excited state by applying the Rehm−Weller formalism[87] (eq 1 from ref 87):

$$\Delta G = F[E^{ox} - E^{red}(MV^{++})] - \Delta E_{0,0} + \Delta E_{coul}$$

The value obtained of 3.1 V vs SCE indicates that $[MV^{2+}]^*$ is an extremely good oxidizing species, much more powerful than in its ground state, as expected. According to eq 1 from ref 87, single electron transfer to $[MV^{2+}]^*$ will be thermodynamically favored for those donor sites of the zeolite with redox potential lower than 3.1 V. The fact that $MV^{\bullet+}$ is generated in all the zeolites proves experimentally that sites compatible with this redox potential do exist.

We propose that the electron donor sites are the oxygens of the framework based on the following grounds: (i) the present knowledge of the zeolite structure that points to bridging Si−O−Al oxygens as the higher electron density sites of the framework; (ii) the insensitivity of the initial single electron-transfer step leading to $MV^{\bullet+}$ to the nature of the associated cation; (iii) the absence of detectable extraframework polyoxoaluminates by IR in NaY, where $MV^{\bullet+}$ is nevertheless generated; (iv) the amount of $MV^{\bullet+}$ that can be formed as estimated by the reported extinction coefficients of MV^{2+} and $MV^{\bullet+}$ in solution being too high to be related to defects of the lattice for highly crystalline samples such as those employed here.

Finally, as we have previously mentioned, during XPS analysis of the MV^{2+}-doped zeolites, X-ray irradiation results in development of a blue color that could be indicative of the generation of $MV^{\bullet+}$. Taking into account the greater ability of CsNaY to stabilize this radical cation, we carried out an XPS study of MV−CsNaY in order to establish the presence of $MV^{\bullet+}$. A comparison of the results obtained for different samples is given in Figure 11; despite the poorer signal-to-noise, the blue MV−CsNaY sample presents two resolved nitrogen peaks at 399.7 and 402.5 eV that we assign to the radical and positive nitrogens of $MV^{\bullet+}$, respectively. The peak at lower energy is not significant for the MV−MCM-41 (Figure 11C) or MV−NaZSM-5 (not included in Figure 11) samples, showing that the efficiency of the single electron donor of CsNaY is higher than for the other MV-doped zeolites. We noticed that there is a shift in the values of the nitrogen 1s electron energies going from crystals of $MVCl_2$ to MV incorporated inside the zeolite voids. Although these variations in XPS are well documented, they can be due to differences in stability and molecular interaction of MV^{2+} when it is located inside the rigid cavitites of the zeolite or when placed in the lattice of pure $MVCl_2$ crystals. In the latter case, the possibility that aggregation or complexation with Cl^- profoundly influences the XPS measurements should be considered.

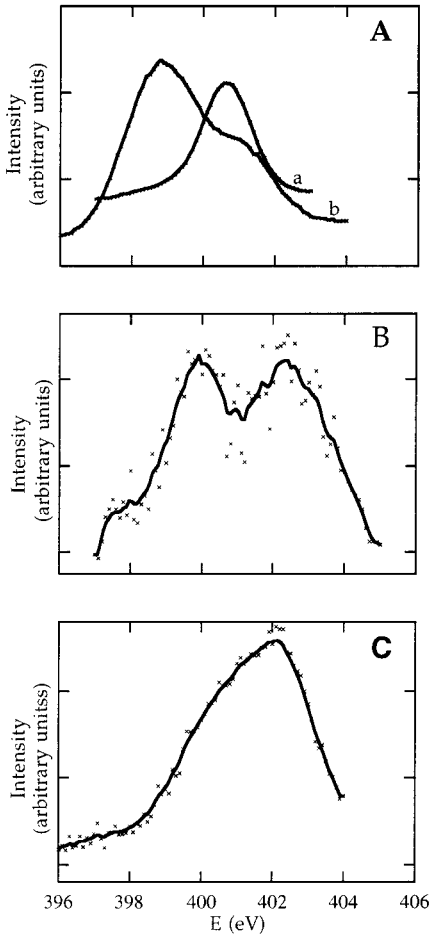

Figure 11. (A) Nitrogen peaks of the XPS spectra of $MVCl_2$ at low-power (80 W) (a) and high-power irradiation (240 W, after 60 min exposure) (b), as well as high-power irradiation (240 W, 5 min exposure) for MV−CsNaY (B) and MV-MCM-41 (C). The curves correspond to smooth fits of the experimental points. The maximum at 402.5 eV is assigned to positive N, while the lower energy peak at 399.5 is attributed to a N radical.

Conclusions

We have shown that absorption of MV^{2+} in zeolites by ion exchange leads to MV^{2+} as the only absorbate. No other species can be detected by XPS, IR, or Raman spectroscopy. Some of the molecular properties of MV^{2+}, particularly fluorescence, are sensitive to the nature of the zeolitic host. By observing that $MV^{\bullet+}$ is photogenerated in all cases, we have provided direct evidence that zeolites can behave as single electron donors. By following the decay of $MV^{\bullet+}$, we have established a relationship between the framework basicity of zeolites and the rate constant of the back-electron transfer, with $MV^{\bullet+}$ being longest-lived in Cs-exchanged zeolites.

Experimental Section

NaX and NaY were commercial samples (Aldrich 13X molecular sieves and Union Carbide SK-40, respectively). Acidic HNaY was obtained starting from NaY by exhaustive Na^+-to-NH_4^+ ion exchange using aqueous solutions of ammonium acetate followed by deep bed calcination using the experimental protocol previously reported.[88] Alkaline ion-exchanged Y zeolites were prepared by stirring at room temperature a suspension of NaY in 0.2 M aqueous solutions of the corresponding nitrate salts using a solid-to-liquid ratio of 1:10. The resulting partially exchanged samples were submitted to two additional exchange cycles, but using 0.4 and 0.6 M aqueous solutions of the corresponding nitrates. Hβ was obtained by template decomposition (823 K, 5 h) of the as-synthesized tetraethylammonium sample (Si/Al = 13 determined by MAS NMR).[89] The sodium form was obtained by treatment with aqueous 1 M NaCl solution and then subsequently washed with distilled deionized water until the silver ion test for choride was negative. Na−ZSM-5 was obtained directly by template-free synthesis, as reported in the literature.[90] MCM-41 was obtained using hexadecyltrimethylammonium bromide and tetramethylammonium hydroxide as templates according to the method reported.[91] NaMor was a commercial sample (PQ Industries).

Chemical analyses were carried out by quantitative atomic absorption spectroscopy after complete dissociation of the solids with concentrated HF/HNO_3 mixtures at 50 °C. C and N combustion analyses were performed in a Perkin-Elmer analyzer (EA 1108, CHNS-O). Thermogravimetry−differential scanning calorimetry were carried out under an air stream using a Netzch

thermobalance (STA 409) and kaolin as a standard. Ground-state diffuse reflectance spectra were recorded using a Shimadzu UV-2021 PC spectrophotometer with an integrating sphere accessory. Steady-state fluorescence measurements were performed at room temperature with a Perkin-Elmer LS-50 spectrofluorometer equipped with a front-face attachment for solid samples. FT-IR spectra of self-consistent wafers (10 mg) were recorded at room temperature under vacuum using a Nicolet spectrometer coupled with a data station. Prior to recording the IR spectra, the samples were successively outgassed at 10^{-2} Pa at room temperature, 100, 200, and 300 °C for periods of 1 h. The FT-Raman spectra were recorded on a Bio-Rad spectrometer, Model FT-Raman II. The 1.064 μm line of a Nd:YAG laser was used for excitation along with a germanium detector cooled to liquid nitrogen temperature. The Raman spectra of powder samples and the liquid solutions were examined in the 180° scattering configuration using high-quality quartz tubes as cells. The laser power at the samples was ~100 mW. The spectral resolution was about 4 cm^{-1}, and the number of scans varied from 800 to 4000 with recording times from 30 min to 2 h. The Raman spectra were corrected for instrumental response using a white light reference spectrum. XPS measurements were carried out at room temperature with a concentric hemispherical analyzer operated in the constant pass energy mode (50 eV). A Mg Kα X-ray source ($h\nu = 1253.6$ eV) was used. A vacuum ca. 5×10^{-9} Torr was always attained in the analysis chamber during XPS recording. Charging effects were calibrated by the C (1s) line at 284.6 eV. All ^{13}C CP/MAS NMR spectra were acquired on a Brucker ASX-200 solid-state NMR spectrometer operating at 50.3 MHz for ^{13}C. The cross polarization contact times were set to 1 ms, and a 2 s relaxation delay was used. The samples were spun at 4500 Hz.

Fluorescence decays were recorded with a Hamamatsu C-4334 streak scope, which allows simultaneous spectral and time resolution, using a Continuum PY-61 picosecond Nd:YAG laser (355 nm, 35 ps, $\leq$4 mJ $pulse^{-1}$). The time-resolved diffuse reflectance laser setup is similar to those previously described.[78,92,93] Either the fourth or third harmonic from a Surelite Nd:YAG laser (266 or 355 nm, $\leq$10 ns, 20−10 mJ $pulse^{-1}$) was used for excitation. Samples were placed in 3×7 mm^2 Suprasil quartz cells capped with rubber septa and purged with nitrogen for at least 30 min before any laser experiment. For low-intensity steady photolysis the samples were outgassed at 10^{-4} Torr for 12 h in quartz tubes of 5 mm of diameter and sealed before irradiation with medium-pressure 125 Hg lamps for 30 min.

Acknowledgment. Financial support by the Canadian NSERC through a research grant (J.C.S.) and the Spanish DGICYT (H.G., Project PB93-047) is gratefully acknowledged. Partial funding by the European Comission (Contract CHR-CT93-0280) is also acknowledged. J.C.S. is the recipient of a Killam fellowship awarded by the Canada Council. S.G. also thanks to the Spanish Ministerio de Educación y Ciencia for a scholarship. We are indebted to Mrs. Nadereh Mohtat for her assistance in the picosecond laser measurements, to Dr. G. A. Facey for performing MAS ^{13}C-NMR spectra, and to Dr. V. Fornés and Mrs. R. Torrero for recording the IR spectra.

References and Notes

(1) Ramamurthy, V.; Caspar, J. V.; Corbin, D. R. *J. Am. Chem. Soc.* **1991**, *113*, 594.
(2) Rhodes, C. J. *J. Chem. Soc., Faraday Trans.* **1991**, *87*, 3179.
(3) Rhodes, C. J.; Standing, M. *J. Chem. Soc., Perkin Trans. 2* **1992**, 1455.
(4) Rhodes, C. J.; Reid, I. D.; Roduner, E. *J. Chem. Soc., Chem. Commun.* **1993**, 512.
(5) Rhodes, C. J. *Colloids Surf. A* **1993**, *72*, 111.
(6) Rhodes, C. J. In *Annual Report on the Progress of Physical Chemistry*; Royal Society of Chemistry: London, 1993; Vol. 90, p 82.
(7) Chen, F. R.; Fripiat, J. J. *J. Phys. Chem.* **1992**, *96*, 819.
(8) Chen, F. R.; Fripiat, J. J. *J. Phys. Chem.* **1993**, *97*, 5796.
(9) Liu, X.; Iu, K.-K.; Thomas, J. K.; He, H.; Klinowski, J. *J. Am. Chem. Soc.* **1994**, *116*, 11811.
(10) Corma, A.; Fornés, V.; García, H.; Martí, V.; Miranda, M. A. *Chem. Mater.* **1995**, *7*, 2136.
(11) Folgado, J.-V.; García, H.; Martí, V.; Esplá, M. *Tetrahedron*, in press.
(12) Chen, F. R.; Fripiat, J. J. In *Ninth International Zeolite Conference*; Butterworth-Heinemann: Montreal, 1992; p 603.
(13) Yoon, K. B. *Chem. Rev. (Washington, D.C.)* **1993**, *93*, 321.
(14) Cozens, F. L.; García, H.; Scaiano, J. C. *Langmuir* **1994**, *10*, 2246.
(15) Brun, A. M.; Hubig, S. M.; Rodgers, M. A. J.; Wade, W. H. *J. Phys. Chem.* **1992**, *96*, 710.
(16) Endo, T.; Saotome, Y.; Okawara, M. J. *J. Am. Chem. Soc.* **1984**, *106*, 1124.
(17) Endo, T.; Ageishi, K.; Okawara, M. *J. Org. Chem.* **1986**, *51*, 4309.
(18) Goren, Z.; Willner, I. *J. Am. Chem. Soc.* **1983**, *105*, 7764.
(19) Hamity, M.; Lema, R. H. *Can. J. Chem.* **1991**, *69*, 146.
(20) Hamity, M.; Lema, R. H. *J. Photochem. Photobiol. A* **1993**, *76*, 83.
(21) Katakis, D. F.; Mitsopoulou, C.; Konstanatatos, J.; Vrachnou, E.; Falaras, P. *J. Photochem. Photobiol. A* **1992**, *68*, 375.
(22) Maidan, R.; Goren, Z.; Becker, J. Y.; Willner, I. *J. Am. Chem. Soc.* **1984**, *106*, 6217.
(23) Mandler, D.; Willner, I. *J. Am. Chem. Soc.* **1984**, *106*, 5352.
(24) Mcmanus, H. J. D.; Finel, C.; Kevan, L. *Radiat. Phys. Chem.* **1995**, *45*, 761.
(25) Ebbesen, T. W.; Ferraudi, G. *J. Phys. Chem.* **1983**, *87*, 3717.
(26) Evans, A. G.; Dodson, N. K.; Rees, N. H. *J. Chem. Soc., Perkin. Trans.* **1976**, *2*, 859.
(27) Garg, B. S.; Pardeep, N. *Indian J. Chem., Sect. A: Inorg., Phys., Theor., Anal.* **1993**, *32*, 601.
(28) Kaifer, A. E.; Quintela, P. A.; Schuette, J. M. *J. Inclusion Phenom. Mol. Recognit. Chem.* **1989**, *7*, 107.
(29) Komers, K. *J. Chem. Res., Synop.* **1994**, 293.
(30) Lee, C.; Kim, C.; Park, J. W. *J. Electroanal. Chem.* **1994**, *374*, 115.
(31) Lu, T.; Cotton, T. M.; Hurst, J. K.; Thompson, D. H. P. *J. Phys. Chem.* **1988**, *92*, 6978.
(32) Mao, Y.; Breen, N. E.; Thomas, J. K. *J. Phys. Chem.* **1995**, *99*, 9909.
(33) Misono, Y.; Shibasaki, K.; Yamasawa, N.; Mineo, Y.; Itoh, K. *J. Phys. Chem.* **1993**, *97*, 6054.
(34) Mizuguchi, J.; Karfunkel, H. *Ber. Bunsen-Ges. Phys. Chem.* **1993**, *97*, 1466.
(35) Tang, X. Y.; Schneider, T.; Buttry, D. A. *Langmuir* **1994**, *10*, 2235.
(36) Wolkers, H.; Stegmann, R.; Frenking, G.; Dehnicke, K.; Fenske, D.; Baum, G. *Z. Naturforsch. B* **1993**, *48*, 1341.
(37) Xiang, B. S.; Kevan, L. *J. Phys. Chem.* **1994**, *98*, 5120.
(38) Kosower, E. M.; Cotter, J. L. *J. Am. Chem. Soc.* **1964**, *86*, 5524.
(39) Meier, W. M.; Olson, D. H. *Atlas of Zeolite Structure Types*; Butterworth: London, 1992.
(40) Beck, J. S.; Vartuli, J. C.; Roth, W. J.; Leonowicz, M. E.; Kresge, C. T.; Schmitt, K. D.; Chu, C. T.-W.; Olson, D. H.; Sheppard, E. W.; McCullen, S. B.; Higgins, J. B.; Schlenker, J. L. *J. Am. Chem. Soc.* **1992**, *114*, 10834.
(41) Behrens, P. *Adv. Mater.* **1993**, *5*, 127.
(42) Behrens, P.; Haak, M. *Angew. Chem., Int. Ed. Engl.* **1993**, *32*, 696.
(43) Corma, A.; Fornés, V.; Martín-Aranda, R. M.; García, H.; Primo, J. *Appl. Catal.* **1990**, *59*, 237.
(44) Hattori, H. *Chem. Rev. (Washington, D.C.)* **1995**, *95*, 537.
(45) Koller, H.; Burger, B.; Schneider, A. M.; Engelhardt, G.; Weitkamp, J. *Microporous Mater.* **1995**, *5*, 219.
(46) Barthomeuf, D. *J. Phys. Chem.* **1984**, *88*, 43.
(47) Huang, M.; Adnot, A.; Kaliaguine, S. *J. Catal.* **1992**, *137*, 322.
(48) Huang, M. M.; Kaliaguine, S. *J. Chem. Soc., Faraday Trans.* **1992**, *88*, 751.
(49) Huang, M. M.; Kaliaguine, S.; Muscas, M.; Auroux, A. *J. Catal.* **1995**, *157*, 266.
(50) Kustov, L. M.; Kazansky, V. B. *J. Chem. Soc., Faraday Trans.* **1991**, *87*, 2675.
(51) Lasperas, M.; Rodriguez, I.; Brunel, D.; Cambon, H.; Geneste, P. *Stud. Surf. Sci. Catal.* **1995**, *97*, 319.
(52) Uvarova, E. B.; Kustov, L. M.; Kazansky, V. B. *Stud. Surf. Sci. Catal.* **1995**, *94*, 254.
(53) Veloso, C. O.; Monteiro, J. L. F.; Sousaaguiar, E. F. *Stud. Surf. Sci. Catal.* **1994**, *84*, 1913.
(54) Barrer, R. M. *Zeolites and Clay Minerals as Sorbents and Molecular Sieves*; Academic Press: London, 1978.
(55) Breck, D. W. *Zeolite Molecular Sieves: Structure, Chemistry and Use*; John Wiley and Sons: New York, 1974.

(56) *Introduction to Zeolite Science and Practice*; van Bekkum, H., Flanigen, E. M., Jansen, J. C., Eds.; Elsevier: Amsterdam, 1991.
(57) Yoon, K. B.; Kochi, J. K. *J. Am. Chem. Soc.* **1989**, *111*, 1128.
(58) Yoon, K. B.; Park, Y. S. *J. Chem. Soc., Chem. Commun.* **1993**, 522.
(59) Yoon, K. B.; Huh, T. J.; Corbin, D. R.; Kochi, J. K. *J. Phys. Chem.* **1993**, *97*, 6492.
(60) Yoon, K. B.; Huh, T. J.; Kochi, J. K. *J. Phys. Chem.* **1995**, *99*, 7042.
(61) Calzaferri, G.; Lanz, M.; Li, J.-w. *J. Chem. Soc., Chem. Commun.* **1995**, 1313.
(62) Alvaro, M.; García, H.; García, S.; Fernández, L. *Tetrahedron Lett.* **1996**, *37*, 2873.
(63) Hydrolysis of solvated di- and trivalent cations to generate adventitious protons $[M(H_2O)_x^{n+} \leftrightarrow M(H_2O)_{x-1}(OH)^{(n+1)+} + H^+]$ is a common process to split positive charges over different positions of the lattice.
(64) Corma, A.; Zicovich-Wilson, C.; Viruela, P. *J. Phys. Chem.* **1994**, *98*, 10863.
(65) Zicovich-Wilson, C.; Planelles, J. H.; Jaskolski, W. *Int. J. Quantum Chem.* **1994**, *50*, 429.
(66) Zicovich-Wilson, C. M.; Corma, A.; Viruela, P. *J. Phys. Chem.* **1994**, *98*, 10863.
(67) Corma, A.; García, H.; Sastre, G.; Viruela, P. M. *J. Phys. Chem.*, submitted.
(68) Alvaro, M.; Facey, G. A.; García, H.; García, S.; Scaiano, J. C. *J. Phys. Chem.* **1996**, *100*, 18173.
(69) Mau, A. W.-H.; Overbeek, J. M.; Loder, J. W.; Sasse, W. H. F. *J. Chem. Soc., Faraday Trans. 2* **1986**, *82*, 868.
(70) Villemure, G.; Detellier, C.; Szabo, A. G. *J. Am. Chem. Soc.* **1986**, *108*, 4656.
(71) Villemure, G.; Detellier, C.; Szabo, A. G. *Langmuir* **1991**, *7*, 1215.
(72) Kuczynski, J. P.; Milosavljevic, B. H.; Lappin, A. G.; Thomas, J. K. *Chem. Phys. Lett.* **1984**, *104*, 149.
(73) Cammenga, H. K.; Epple, M. *Angew. Chem., Int. Ed. Engl.* **1995**, *34*, 1171.
(74) Silverstein, R. M.; Bassler, G. C.; Morrill, T. C. *Spectroscopic Identificationm of Organic Compounds*, 4th ed.; John Wiley: New York, 1981.
(75) Schrader, B. *Infrared and Raman Spectroscopy (Methods and Applications)*; VCH Publishers Inc: Weinheim, 1995.
(76) Forster, M.; Girling, R. B.; Hester, R. E. *J. Raman Spectrosc.* **1982**, *12*, 36.
(77) Schoonover, J. R.; Chen, P. Y.; Bates, W. D.; Dyer, R. B.; Meyer, T. J. *Inorg. Chem.* **1994**, *33*, 793.
(78) Bohne, C.; Redmond, R. W.; Scaiano, J. C. In *Photochemistry in Organized and Constrained Media*; Ramamurthy, V., Ed.; VCH: New York, 1991; Chapter 3.
(79) Cozens, F. L.; Régimbald, M.; García, H.; Scaiano, J. C. *J. Phys. Chem.* **1996**, *100*, 18165.
(80) Park, J. W.; Choi, N. H.; Kim, J. H. *J. Phys. Chem.* **1996**, *100*, 769.
(81) Adar, E.; Degani, Y.; Goren, Z.; Willner, I. *J. Am. Chem. Soc.* **1986**, *108*, 4696.
(82) Barna, G. G.; Fish, J. G. *J. Electrochem. Soc.* **1987**, *128*, 1290.
(83) Yasuda, A.; Mori, H.; Seto, J. *J. Appl. Electrochem.* **1987**, *17*, 567.
(84) Evans, A. G.; Evans, J. C.; Baker, M. W. *J. Am. Chem. Soc.* **1977**, *99*, 5882.
(85) Claude-Montigni, B.; Merlin, A.; Tondre, C. *J. Phys. Chem.* **1992**, *96*, 4432.
(86) Scaiano, J. C.; Johnston, L. J.; McGimpsey, W. G.; Weir, D. *Acc. Chem. Res* **1988**, *21*, 22.
(87) Rehm, D.; Weller, A. *Ber. Bunsen-Ges. Phys. Chem.* **1969**, *73*, 834.
(88) Corma, A.; García, H.; Iborra, S.; Primo, J. *J. Catal.* **1989**, *120*, 78.
(89) Pérez-Pariente, J.; Martens, J.; Jacobs, P. A. *Appl. Catal.* **1987**, *31*, 35.
(90) Argauer, R. J.; Landlolt, G. R. U.S. Patent 3 702 886, 1982.
(91) Corma, A.; Fornés, V.; Navarro, M. T.; Pérez-Pariente, J. *J. Catal.* **1994**, *148*, 569.
(92) Kelly, G.; Willsher, C. J.; Wilkinson, F.; Netto-Ferreira, J. C.; Olea, A.; Weir, D.; Johnston, L. J.; Scaiano, J. C. *Can. J. Chem.* **1990**, *68*, 812.
(93) Wilkinson, F.; Kelly, G. In *Handbook of Organic Photochemistry*; Scaiano, J. C., Ed.; CRC Press: Boca Raton, FL, 1989; Vol. 1, p 293.